The Astrophysical Journal Letters, 983:L26 (8pp), 2025 April 10 https://doi.org/10.3847/2041-8213/adc5e3


# Lack of Rest-frame Ultraviolet Variability in Little Red Dots Based on HST and JWST Observations

Wei Leong Tee[1], Xiaohui Fan[1], Feige Wang[1,2], and Jinyi Yang[1,2]
[1] Steward Observatory, University of Arizona, 933 N Cherry Ave, Tucson, AZ 85719, USA
[2] Department of Astronomy, The University of Michigan, 1085 S. University, 323 West Hall, Ann Arbor, MI 48109-1107, USA
*Received 2024 December 5; revised 2025 February 7; accepted 2025 March 2; published 2025 April 9*

## Abstract

Variability is a fundamental signature for active galactic nuclei (AGN) activity and serves as an unbiased indicator for rapid instability happening near the center of supermassive black holes (SMBHs). Previous studies showed that AGN variability does not have strong redshift evolution, and scales with their bolometric luminosity and BH mass, making it a powerful probe to identify low-mass, low-luminosity AGNs at high redshift. JWST has discovered a new population of high-redshift galaxies likely hosting moderate accreting BHs ($>10^6 M_\odot$)—the little red dots (LRDs; $z \sim 4$–10). In this Letter, we study the variability of a sample of 22 LRDs with V-shaped spectral energy distributions in three JWST deep fields that also have reliable Hubble Space Telescope observations in closely paired filters at 1–2 $\mu$m (rest-frame UV), with the time difference between 6 and 11 yr. This LRD sample covers a redshift range of $3 < z < 8$ with $-21.3 < M_{\rm UV} < -18.4$. Based on both photometry and imaging difference analyses, we find a mean magnitude difference of $\sim 0.15 \pm 0.26$ mag, with none of the LRDs showing photometric variability at $3\sigma$ significance. Extrapolation of Sloan Digital Sky Survey quasar variability predicts a magnitude change of order 0.3 mag for our LRD sample. This suggests an upper limit of about ~30% AGN contribution to the total observed UV light in our sample of LRDs.

*Unified Astronomy Thesaurus concepts:* Active galactic nuclei (16); Supermassive black holes (1663); Quasars (1319)

## 1. Introduction

Early JWST observations have discovered a class of compact galaxies showing "V-shaped" spectral energy distribution (SED) with blue UV excess and rapidly raising red optical-to-IR continuum—usually referred to as the little red dots (LRDs), with strong indication of active galactic nuclei (AGN) activities, especially for a subset of that exhibit rest-frame optical broad-line (BL) emissions ($>1000\,{\rm km\,s^{-1}}$, $M_{\rm BH} = 10^{6-8}\,M_\odot$, and $L_{\rm bol} \sim 10^{46}\,{\rm erg\,s^{-1}}$; Y. Harikane et al. 2023a; D. D. Kocevski et al. 2023; J. E. Greene et al. 2024; R. Maiolino et al. 2024a; J. Matthee et al. 2024; I. Labbe et al. 2025). Their clear BL detection and compact red IR continuum emission are suggestive of rapid accreting supermassive black hole (SMBH) activity; however, their blue UV spectra are more consistent with star-forming galaxies (M. Killi et al. 2024), with a potential small contribution from AGN-scattered light (J. E. Greene et al. 2024; J. Matthee et al. 2024). In addition, the absence of strong detection in LRDs' X-ray stacking analysis (M. Yue et al. 2024) has questioned their AGN origin. Although several theories have been proposed in attempt to explain the AGN signatures (e.g., R. Maiolino et al. 2024b; Z. Li et al. 2025), the majority of LRDs have blue UV slope that is hardly consistent with purely AGN radiation, with reported AGN flux fraction ranging from 40% to 80% through morphology and SED determinations (Y. Harikane et al. 2023a; E. Durodola et al. 2024). An independent test will further constrain the boundary of AGN contribution.



AGNs are known to vary in brightness (>0.1 mag) with timescales ranging from days to years. It is thought to originate from the instability in the accretion disk close to the SMBH; therefore, a hallmark of AGN phenomena. Extensive research have been conducted for low-redshift quasar/AGN variability in X-ray, UV, and optical wavelengths (e.g., T. J. Turner et al. 1999; D. E. Vanden Berk et al. 2004; C. L. MacLeod et al. 2012). The structure function (SF), a power spectrum density measurement of AGN magnitude change over time, is well-described with a time-series damped-random walk (DRW) model, with a characteristic variability amplitude $\rm SF_\infty$ and turnover timescale $\tau$ (e.g., C. L. MacLeod et al. 2012; S. Kozłowski 2016). Given the anticorrelation of rest UV/optical luminosity with variability amplitude (T. Simm et al. 2016), rest-frame UV-optical variability become a powerful tool to discover and study high-redshift faint AGNs, which may hold a key to constraining SMBH seeding models (K. Inayoshi & K. Ichikawa 2024; J. Jeon et al. 2025), the AGN contribution to reionization at cosmic dawn (S. L. Finkelstein et al. 2019; P. Dayal et al. 2020; L. Y. A. Yung et al. 2021), and the early coevolution of galaxies and SMBHs (M. Habouzit et al. 2022; K. Inayoshi et al. 2022; F. Pacucci et al. 2023). If the rest-frame UV radiation of LRDs is dominated by AGN emission, they are expected to show strong variability at this wavelength.

However, the variability study of high-redshift, low-luminosity AGNs is challenging due to a combination of time dilation and their faintness in the rest-frame UV, which is now redshifted into the red optical and near-infrared (NIR) wavelengths. P. Sánchez et al. (2017) reported 10%–20% NIR variable sources in 1.4 $\rm deg^2$ COSMOS are AGNs ($M_Y \leqslant -22$ at $z = 1$–3). Similar studies at $z > 4$ are not feasible before the JWST launch. JWST and Hubble Space Telescope (HST) have similar pairs of filters at 1–2, $\mu$m, allowing for the direct study of photometric variations between

new JWST observations and previous HST observations of the same field over a time span of 6–11 yr. This makes them ideal for searching for variable AGNs at $z > 3$. As an example, R. O'Brien et al. (2024) searched for transients using two epochs high resolution HST imaging in the JWST time-domain field, and found a dozen brown dwarfs and $z \lesssim 3$ variable AGN candidates. M. J. Hayes et al. (2024) conducted a high-redshift transients search in HUDF using two epochs of HST photometric data and successfully identified two intermediate redshift AGNs and two reionization era quasar candidates (but see C. DeCoursey et al. (2025), which suggests that one of them is likely a late type star).

In this Letter, we study the rest-frame UV variability of a sample of LRDs identified in the JWST deep field observations with existing HST observations in closely matched filter pairs. We first introduce the methodology of the variable source finder in Section 2. We describe the use of publicly available images/catalogs, data preparation, and the LRD sample definition in Section 2.1. In Section 3, we present the constraints on photometric variabilities of LRDs and their implications on the AGN nature of LRDs. We use AB magnitude throughout this work. Errors are quoted within 68% confidence interval, and assume a flat ΛCDM cosmology with $H_0 = 70\,\mathrm{km\,s^{-1}\,Mpc^{-1}}$, $\Omega_m = 0.3$, and $\Omega_\Lambda = 0.7$.

## 2. Methodology

### 2.1. Imaging Data and Photometry

We study the variability of LRDs selected from three deep fields with both HST and JWST observations: Extended Groth Strip (EGS),[3] Great Observatories Origins Deep Survey South (GOODS-S),[4,5] and Abell 2744 (A2744). The basic properties of these imaging data set are summarized in Table 1.

In order to carry out consistent photometric measurements and image subtractions, all image mosaics have been registered to the Gaia reference frame, and the HST mosaics have been resampled to the common tangential plane as with the JWST image and common pixel scales of $0\farcs03\,\mathrm{pixel^{-1}}$ For EGS and GOODS-S images, we do point-spread function (PSF)-matching for JWST images to HST/F160W because the latter has the broadest full width at half-maximum (FWHM) in 1–2 $\mu$m, photometry extraction and estimation are done on low-resolution HST and JWST images. More details regarding data preparation can be found in W. L. Tee et al. (2025, in preparation).

### 2.2. Photometry Calibration

Both HST and JWST have similar filter coverage over 1–2 $\mu$m, i.e., F125W and F160W with HST's Wide Field Camera 3 (WFC3; $5\sigma \sim$26–27 mag), and F115W and F150W by JWST's Near Infrared Camera (NIRCam; $5\sigma \sim$28–29 mag). Given the fact that JWST/NIRCam imaging depth is, in general, 2 mag deeper than HST/WFC3, we can use the higher quality JWST magnitudes to color calibrate the HST magnitudes and account for the small filter differences. We choose a simple color correction model for HST magnitude using JWST magnitude and color,

$$m_{\mathrm{HST}} = \beta + m_{\mathrm{JWST}} + \alpha \times (m_{\mathrm{F115W}} - m_{\mathrm{F150W}}). \quad (1)$$

The calibrated HST photometry, $m_{\mathrm{HST_{exp}}}$, namely expected HST photometry based on JWST observations, should compare with the measured value $m_{\mathrm{HST}}$. We choose to adopt aperture photometry for the calibration since our goal is to study variable AGNs, in which the brightness should only change at the galactic centers. If a source is detected in JWST filters but becomes significantly brighter or fainter in HST filters, it will be classified as a potential variable AGN. We use a $0\farcs5$ aperture size ($0\farcs48$ in UNCOVER catalog) for aperture flux estimation, about 2 times larger than HST/F160W PSF FWHM ($\sim 0\farcs22$; W. L. Tee et al. 2025, in preparation; M. B. Bagley et al. 2023). The photometric uncertainties are estimated by randomly placing apertures within survey areas, masking out detected sources. We construct a sample of field sources with good photometry, size, and redshift measurements. We measure and compare their observed HST magnitudes with JWST-calibrated HST magnitudes to validate the robustness. The systematic offset is <0.01 mag, with $\sigma_{\mathrm{calib}} = 0.05$ (W. L. Tee et al. 2025, in preparation), and the result does not change when we inspect individual spectroscopically confirmed sources. We consider this 5% calibration error as the uncertainty floor in the flux error measurement in this work. The measured value of the correction terms are $(\alpha,\ \beta)_{\mathrm{F125W}} = (0.0068,\ -0.278)$ and $(\alpha,\ \beta)_{\mathrm{F160W}} = (0.0067,\ -0.014)$, respectively.

### 2.3. Variable Source Classification

We define $f_{\mathrm{obs}}$ as measured HST band aperture flux, $f_{\mathrm{exp}}$ as expected aperture flux measured by JWST in HST band, and $\sigma_{\mathrm{obs}}$ and $\sigma_{\mathrm{exp}}$ are aperture flux errors following a similar definition. Photometric variability in the flux space, $\mathrm{var}_p$, is characterized as

$$\mathrm{var}_{p,b} = \frac{f_{\mathrm{exp}} - f_{\mathrm{obs}}}{\sqrt{\sigma_{\mathrm{exp}}^2 + \sigma_{\mathrm{obs}}{}^2}}, \quad (2)$$

where $p$ stands for photometry method, $b =$ HST/F125W, HST/F160W. A source is considered variable if $\mathrm{var}_{p,b} > 3$.

Pure aperture photometry selection may include contamination from supernovae, which are off-centered, or moving transients. We also construct a difference image to validate the nature of variability. We create $20'' \times 20''$ JWST/F115W, HST/F125W, JWST/F150W, and HST/F160W cutouts for each source, and scale the JWST cutout flux level to the HST cutout. After preparation of the background-subtracted photometry and astrometry aligned cutouts, we use the PyZOGY[6] prescription (B. Zackay et al. 2016; D. Guevel et al. 2021), which calculate the difference image $D$ given input pair images and corresponding PSFs, i.e., (JWST/F115W, HST/F125W) and (JWST/F150W, HST/F160W). We measure the flux difference $\Delta f_D$ within the aperture directly from difference image $D$, and evaluate the imaging difference variability, $\mathrm{var}_D$, as

$$\mathrm{var}_{D,b} = \frac{\Delta f_{D,b}}{\sqrt{\sigma_{\mathrm{exp}}^2 + \sigma_{\mathrm{obs}}{}^2}}, \quad (3)$$

where $b =$ HST/F125W,F160W, assuming no other dominant noise component present. B. Zackay et al. (2016) showed that

[3] doi: 10.17909/z7p0-8481 (S. Finkelstein et al. 2023).
[4] doi: 10.17909/fsc4-dt61 (C. Williams et al. 2023).
[5] doi: 10.17909/8tdj-8n28 (M. Rieke et al. 2023).
[6] https://github.com/dguevel/PyZOGY

**Table 1**
Field Information Where LRDs Are Selected

| Field | $5\sigma$ Depth ($d \sim 0.''3$) | | | | $T_{\rm HST}$ | Overlapped | | | References |
|---|---|---|---|---|---|---|---|---|---|
| | JWST F115W | HST F125W | JWST F150W | HST F160W | | $T_{\rm JWST}$ | Area (arcmin$^2$) | Related Surveys | |
| EGS | 27.3 | 27.0 | 27.0 | 27.1 | 2012.14 | 2022.82 | 188 | HST/CANDELS<br>JWST/CEERS | N. A. Grogin et al. (2011), A. M. Koekemoer et al. (2011), M. B. Bagley et al. (2023), and W. L. Tee et al. (2025, in preparation) |
| GOODS-S | 29.3 | 27.9 | 29.3 | 27.6 | 2011.29 | 2023.19 | 159 | HST/HLF<br>JWST/JADES | G. Illingworth et al. (2016), K. E. Whitaker et al. (2019), D. J. Eisenstein et al. (2023), and W. L. Tee et al. (2025, in preparation) |
| A2744 | 28.2 | 27.1 | 28.2 | 26.5 | 2016.03 | 2023.21 | 148 | HST/BUFFALO, HFF<br>JWST/UNCOVER, MegaScience | J. R. Weaver et al. (2024) and K. A. Suess et al. (2024) |

$D$ image is a proper difference image, where the noise level is dominated by white noise only given a reasonable fit to the flux zero-points in pair images. We use both $\mathrm{var}_{p,b}$ and $\mathrm{var}_{D,b}$ to justify the variable nature of variable sources.

### 2.4. LRD Sample Definition

V. Kokorev et al. (2024) constructed a sample of LRDs at $z = 4$–$9$, selected by their JWST colors and compact sizes. D. D. Kocevski et al. (2024) further characterized the LRD selection by including $\beta_{\mathrm{UV}}$ slope and $\beta_{\mathrm{opt}}$ to select primarily "V-shaped" SED, with or without broad Balmer line detections in publicly available spectroscopic data. They reported a total of 341 $z \sim 2$–$11$ LRDs in JWST public extragalactic surveys, including CEERS (EGS), PRIMER (UDS and COSMOS), JADES (GOODS-S/N), UNCOVER (A2744), and NGDEEP (HUDF) programs. In this work, we focus our study on NIRCam short wavelength (SW) data to characterize the high-redshift LRDs rest-frame near-UV variability, using mainly CEERS, JADES, and UNCOVER data, where public data are officially released. The data preparation detail on EGS and GOODS-S imaging and catalog products will be addressed in W. L. Tee et al. (2025, in preparation). For A2744, we use the images and catalog generated by the UNCOVER team for variability analysis (R. Bezanson et al. 2024; K. A. Suess et al. 2024; J. R. Weaver et al. 2024).

The median JWST/F444W magnitude of LRDs is about 26 mag, but they are fainter in rest-frame UV to about 28.5 mag, which is close to the detection limit in JWST/F115W and JWST/F150W, 1–2 mag deeper than the depth typically of the available HST/F125W and HST/F160W imaging. We use the following three selection criteria to create a sample of LRDs suitable for variability studies: 1. The source is $5\sigma$ detected in JWST/F115W and JWST/F150W, and has mutual image coverage in HST/F125W and HST/F160W. 2. The color-calibrated $f_{\mathrm{exp}}$ in the corresponding HST observations is 3 times above HST noise $\sigma_{\mathrm{obs}}$. This way, if the source is not varying, it has been detected in either epoch. Thus, the selection is not biased against high variable sources that are not detected in HST imaging as a result of their variability. 3. We limit the redshift $z < 8$ to avoid Ly$\alpha$ drop out affecting the calibration between JWST/F115S and HST/F125W bands. The initial catalog consists of 143 LRDs in three fields, which later reduces to 22 sources (15% of the original sample) for a flux-limited sample spanning $-21.23 < M_{\mathrm{UV}} < -18.47$. This sample includes eight BLAGNs (one without BH mass measurements) identified in the literature (Y. Harikane et al. 2023a; J. E. Greene et al. 2024; D. D. Kocevski et al. 2024; R. Maiolino et al. 2024a). We extract their photometry in low-resolution PSF-matched images and calculate their expected HST fluxes and flux errors. Next, we perform imaging difference on photometrically and astrometrically aligned images. Finally, we derive $\mathrm{var}_p$ by calculating the significance between expected flux and measured flux, $\mathrm{var}_D$ by measuring the flux residual significance in difference image $D$.

## 3. Result and Discussion

The redshift and luminosity distribution of all LRDs in the parent sample are displayed in Figure 1, along with $z > 5.5$ faint quasars (X. Fan et al. 2023). We highlight the 22 LRDs/8 BLAGN in this study. Their photometry and variability measurements are reported in Table 2. The majority of the

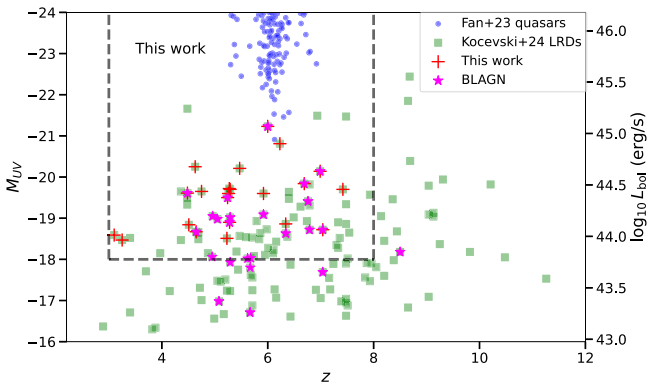


**Figure 1.** Redshift and luminosity distribution of LRDs in the parent sample (green square, $N = 143$; D. D. Kocevski et al. 2024), broad-line AGN subsample (magenta stars), and $z > 5.5$ quasars (blue circle; X. Fan et al. 2023). We construct an unbiased flux-limited sample ($M_{\mathrm{UV}} < -18$) and show the 22 LRDs (8 BLAGNs) considered in this work with red pluses.

sources show $\lesssim$0.2 mag change, as shown in Figure 2. The mean magnitude changes in HST/F125W and HST/F160W are $0.15 \pm 0.26$ and $0.11 \pm 0.23$ mag, respectively.

Several sources show >0.2 mag, noticeably CEERS_1670, CEERS_1669, CEERS_941, CEERS_5208, CEERS_13318, CEERS_24253, and UNCOVER_9497. We calculate their magnitude errors through quadratic sum, $\mathrm{err}_{\Delta m} = \sqrt{\mathrm{err}^2_{\mathrm{obs}} + \mathrm{err}^2_{\mathrm{exp}}}$, where individual magnitude error is derived from the empirical noise function measured by placing fixed radius apertures across random positions in the image (W. L. Tee et al. 2025, in preparation), which already include $\sigma_{\mathrm{calib}}$. We find that the magnitude errors are dominated by shallower HST observations, and none show $>3\sigma$ variability, as shown in Table 2. Our result shows that $\sigma_{\mathrm{non-var}}$ at similar redshift ranges are 0.17 and 0.19 for HST/F125W and HST/F160W (W. L. Tee et al. 2025, in preparation). Comparing the $\sigma_{\mathrm{LRD}} \sim 0.26$ with $\sigma_{\mathrm{non-var}} \sim 0.19$, we do not see significant evidence that LRD are varying sources.

The LRDs in this work are selected via V-shaped SED, among them, eight also show broad H$\alpha$ lines and are hence classified as BLAGN. I. Labbe et al. (2025) show that SEDs of LRDs suggest bolometric luminosities $L_{\mathrm{bol}} = 10^{43-46}$ erg s$^{-1}$, or equivalently $M_{\mathrm{BH}} = 10^{7-9} M_{\odot}$ (J. E. Greene et al. 2024), representing a class of low-medium luminosity AGN hosting overmassive BH at the centers. M. Kokubo & Y. Harikane (2024) reported no variability detected for five broad H$\alpha$ emitters in the GLASS survey, having a median $L_{\mathrm{bol}} = 10^{44}$ erg s$^{-1}$, and a typical BH mass of $M_{\mathrm{BH}} \sim 10^8 M_{\odot}$, a typical LRD sample. To constrain the origin of rest-frame UV emission of LRDs, we compare their asymptotic variability amplitude $\mathrm{SF}_{\infty}$ with the expected value derived from literature studies of variable AGN light curves. Observational $\mathrm{SF}_{\infty}$ is calculated via $\mathrm{SF}_{\infty} = \sqrt{2}\sqrt{\sigma^2_{\mathrm{obs}} - \sigma^2_{\mathrm{non-var}}}$ (C. L. MacLeod et al. 2010), where $\sigma^2_{\mathrm{obs}}$ is the observed magnitude variance, $\sigma^2_{\mathrm{non-var}}$ is the magnitude variance of nonvariable objects in the field with similar time difference. C. L. MacLeod et al. (2010) first determined the dependencies of optical $\mathrm{SF}_{\infty}$ on several AGN properties, including AGN luminosity, redshift, $M_{\mathrm{BH}}$, etc., through modeling the Sloan Digital Sky Survey (SDSS) Stripe 82 quasar light curves as DRW (also see S. Kozłowski 2016). Structure function approaches the $\mathrm{SF}_{\infty}$ when the time difference between two epochs is greater than the characteristic turnover

**Table 2**
Table on LRDs Photometry and Variability

| ID | R.A. | Decl. | $z_{best}$ | $M_{UV}$ (mag) | $\log_{10}(M_{BH})$ ($M_{\odot}$) | $m_{F150W}$ (mag) | $\Delta m_{F125W}$ (mag) | $var_{D,F125W}$ | $\Delta m_{F160W}$ (mag) | $var_{D,F160W}$ | BL Detected | BL and $M_{BH}$ References |
|---|---|---|---|---|---|---|---|---|---|---|---|---|
| JADES_8083 | 03:32:31.88 | −27:48:06.70 | 4.65 | −18.67 | 7.25 | 27.68 ± 0.04 | −0.14 ± 0.28 | 0.58 | −0.02 ± 0.3 | −0.22 | Y | R. Maiolino et al. (2024a) |
| JADES_4454 | 03:32:39.87 | −27:46:19.35 | 6.34 | −18.86 | ⋯ | 28.07 ± 0.07 | 0.02 ± 0.13 | 0.82 | −0.17 ± 0.12 | 2.40 | N | ⋯ |
| JADES_11125 | 03:32:16.24 | −27:48:44.39 | 4.63 | −20.25 | ⋯ | 26.28 ± 0.03 | −0.14 ± 0.08 | 2.47 | −0.19 ± 0.12 | 1.12 | N | ⋯ |
| JADES_20532 | 03:32:29.94 | −27:51:58.68 | 4.51 | −18.84 | ⋯ | 26.27 ± 0.03 | 0.06 ± 0.09 | −1.05 | −0.16 ± 0.12 | 1.26 | N | ⋯ |
| JADES_21925 | 03:32:20.84 | −27:52:23.00 | 3.1 | −18.59 | ⋯ | 27.34 ± 0.03 | 0.02 ± 0.23 | −0.35 | 0.02 ± 0.23 | 0.19 | N | ⋯ |
| JADES_24052 | 03:32:17.79 | −27:53:01.33 | 5.23 | −18.51 | ⋯ | 27.43 ± 0.09 | −0.16 ± 0.4 | 0.55 | 0.01 ± 0.34 | 0.04 | N | ⋯ |
| JADES_26901 | 03:32:23.41 | −27:54:04.52 | 5.26 | −19.6 | ⋯ | 26.44 ± 0.04 | 0.18 ± 0.15 | 1.94 | −0.01 ± 0.27 | −0.12 | N | ⋯ |
| CEERS_397 | 14:19:20.69 | +52:52:57.70 | 6.0 | −21.23 | 7.0 | 26.03 ± 0.04 | 0.12 ± 0.1 | 0.22 | −0.08 ± 0.11 | 0.83 | Y | Y. Harikane et al. (2023a) |
| CEERS_1236 | 14:20:34.87 | +52:58:02.20 | 4.484 | −19.61 | 7.26 | 26.91 ± 0.07 | −0.01 ± 0.21 | 1.26 | 0.02 ± 0.18 | −0.42 | Y | Y. Harikane et al. (2023a) |
| CEERS_1465 | 14:19:33.12 | +52:53:17.70 | 5.274 | −19.72 | ⋯ | 27.09 ± 0.09 | 0.03 ± 0.24 | 0.24 | −0.05 ± 0.29 | 0.17 | N | ⋯ |
| CEERS_1670 | 14:19:17.63 | +52:49:49.01 | 5.242 | −19.5 | 7.62 | 26.63 ± 0.07 | −0.22 ± 0.27 | 1.40 | −0.17 ± 0.19 | 0.95 | Y | Y. Harikane et al. (2023a) |
| CEERS_941 | 14:19:01.91 | +52:50:22.94 | 7.42 | −19.7 | ⋯ | 27.23 ± 0.11 | −0.27 ± 0.48 | 0.65 | −0.19 ± 0.31 | 0.60 | N | ⋯ |
| CEERS_1669 | 14:19:16.25 | +52:52:40.28 | 5.47 | −20.21 | ⋯ | 26.88 ± 0.08 | −0.23 ± 0.32 | 0.85 | 0.08 ± 0.2 | −0.43 | N | ⋯ |
| CEERS_5208 | 14:19:42.54 | +52:56:02.01 | 5.92 | −19.6 | ⋯ | 27.26 ± 0.11 | 0.02 ± 0.32 | 0.65 | −0.21 ± 0.33 | 0.64 | N | ⋯ |
| CEERS_7902 | 14:19:55.93 | +52:57:21.62 | 6.99 | −20.14 | 9.19 | 26.71 ± 0.07 | 0.14 ± 0.26 | −0.61 | 0.06 ± 0.17 | −0.35 | Y | D. D. Kocevski et al. (2024) |
| CEERS_10444 | 14:19:34.14 | +52:52:38.66 | 6.69 | −19.84 | 9.11 | 27.11 ± 0.1 | 0.18 ± 0.3 | −0.25 | −0.09 ± 0.31 | 0.30 | Y | D. D. Kocevski et al. (2024) |
| CEERS_13318 | 14:19:10.89 | +52:47:19.85 | 5.28 | −18.9 | 8.88 | 26.93 ± 0.08 | 0.31 ± 0.23 | −1.23 | −0.07 ± 0.19 | 0.45 | Y | D. D. Kocevski et al. (2024) |
| CEERS_19578 | 14:19:31.24 | +52:48:45.22 | 5.29 | −19.7 | ⋯ | 27.11 ± 0.1 | −0.05 ± 0.35 | 0.03 | −0.09 ± 0.29 | −0.15 | N | ⋯ |
| CEERS_24253 | 14:19:55.19 | +52:51:39.88 | 6.23 | −20.81 | ⋯ | 26.52 ± 0.06 | 0.22 ± 0.16 | −1.88 | 0.06 ± 0.16 | −0.42 | N | ⋯ |
| UNCOVER_9497 | 00:14:19.16 | −30:24:05.65 | 7.04 | −18.72 | 7.3 | 27.96 ± 0.14 | −0.05 ± 0.26 | −0.26 | 0.2 ± 0.2 | −0.75 | N | J. E. Greene et al. (2024) |
| UNCOVER_9447 | 00:14:30.03 | −30:24:05.10 | 3.25 | −18.47 | ⋯ | 24.35 ± 0.02 | −0.1 ± 0.18 | −1.93 | 0.05 ± 0.06 | −2.57 | N | ⋯ |
| UNCOVER_3943 | 00:13:59.72 | −30:21:10.60 | 4.75 | −19.65 | ⋯ | 25.98 ± 0.03 | −0.1 ± 0.24 | 0.09 | 0.07 ± 0.22 | −0.20 | N | ⋯ |

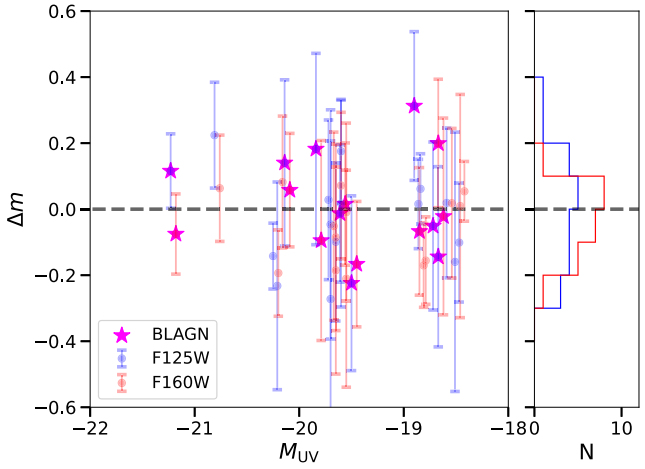


**Figure 2.** Magnitude change between HST and JWST epoch of time difference 6–11 yr. The mean magnitude changes in HST/F125W and HST/F160W are $\sim 0.15 \pm 0.26$ mag.

timescale $\tau$, i.e., entering the white noise regime, which is found to be approximately several hundred days (S. Kozłowski 2016; C. J. Burke et al. 2021). Based on the median 6–11 yr observed time differences between past HST observations and the recent JWST observations, we assume that $SF_\infty$-derived values are indeed the upper limit of the structure function. We adopt the following relation to scale with the rest-frame wavelength ($\lambda_{RF}$) and AGN luminosity ($M_i$) from C. L. MacLeod et al. (2010) (without $M_{BH}$ dependence, see below),

$$\log \mathrm{SF}_\infty = -0.618 - 0.479 \log\left(\frac{\lambda_{RF}}{4000\ \text{Å}}\right) + 0.09(M_i + 23), \quad (4)$$

where $M_i$ is the absolute $i$-band magnitude $K$-corrected to $z = 2$, which is representative of AGN bolometric luminosity ($L_{bol}$) as shown in G. T. Richards et al. 2006). Here we have two options to compute $M_i$: 1. Adopt the $M_{UV}$ computed in D. D. Kocevski et al. (2024) using rest-frame 1450 Å and convert that to $M_i$ using Equation (3) in G. T. Richards et al. (2006). 2. Following Y. Shen et al. (2009), $M_i$ can be characterized with $M_i = 90 - 2.5 \log L_{bol}/\mathrm{erg\ s^{-1}}$, and assuming a fixed $L_{bol}/L_{Edd}$, $M_i$ is a $M_{BH}$ dependent function. The first option assumes a full contribution of UV light from AGN, while the second option is an extrapolation to low-mass AGN from SDSS quasars (C. J. Burke et al. 2023). Note that in our sample, most of the LRDs do not have $M_{BH}$ information, except for the known BLAGNs (Figure 3). We choose to calculate expected $SF_\infty$ with LRDs median $M_{BH}$ of $10^{7.6}\,M_\odot$ within our sample when $M_{BH}$ are not available, and a fixed $L_{bol}/L_{Edd} = 0.1$. We find the expected $SF_\infty$ is >0.3–0.6 mag. Based on what we measured above, a small sample of LRDs gives $SF_\infty \sim 0.25$ mag, which is below the expected variability amplitude.

Note that the first method postulates a model in which full UV light is emitted by AGN (see discussion in J. E. Greene et al. 2024), while the second method assumes a $M_{BH}$-dependent function extrapolated from SDSS Stripe 82 quasars. Fainter, smaller LRDs are subject to having more host galaxy light dilution, resulting in smaller $SF_\infty$ (C. J. Burke et al. 2023). Studies on host-diluted $SF_\infty$ have been conducted extensively, i.e., C. J. Burke et al. (2023, and references therein). In order to obtain a first-order estimation on host galaxy flux contribution, we assume the small flux variation is entirely due to AGN and $\Delta f_{AGN} \ll f_{AGN}$, and the fact that $SF \propto \frac{\Delta f}{f}$. We define the AGN fraction $A$,

$$A = \frac{f_{AGN}}{f_{AGN} + f_{host}} = \frac{\mathrm{SF}_{\infty,d}}{\mathrm{SF}_\infty}, \quad (5)$$

where $SF_{\infty,d}$ and $SF_\infty$ are the host-diluted and normal variability amplitudes, respectively. In our case, observational $SF_\infty$ are treated as $SF_{\infty,d}$. Here we intend to discuss the upper limit of LRDs' UV variability. We drop the magnitude scatter of nonvariable sources and simply compute the upper limit of $SF_{\infty,d}$.

Following the two options to calculate AGN UV light fraction, we compute the mean AGN fraction of the 22 sources in our sample. SDSS quasars have $M_{BH}$ that are 1–2 dex more massive. The fact that $SF_\infty$ scales inversely with $M_{BH}$ ($\log \mathrm{SF}_\infty \propto M_i \propto -\log L_{bol} \propto M_{BH}$) results in a lower limit if extrapolated from the SDSS variability amplitude relation, which we interpret as an upper limit in AGN fraction. Using $M_{BH} = 10^{7.6}\,M_\odot$ and $M_{UV} = -19.6$, we find that the average upper limit of AGN fraction in our sample is ~30%. In other words, AGN can contribute at most one-third of the total fluxes in the LRD rest-frame UV. We show the overall result in Figure 3. Our result is, in general, lower than those reported in the literature with SED analysis on faint AGNs and LRDs at a similar redshift range. Y. Harikane et al. (2023b) reported a contribution of ~50% using faint BLAGNs, while E. Durodola et al. (2024) measured 40%–85% AGN contribution in LRDs spectra. We emphasize that the low AGN UV contribution to LRDs is not conclusive for all LRDs, as some LRDs show not only tentative photometric variability (Z. Zhang et al. 2024), and also significant equivalent width variation (L. J. Furtak et al. 2025). Clearly, a larger sample with multiepoch deep JWST data will benefit the variability studies and provide better constraints on the AGN origin of LRDs' rest-UV spectra, or a non-AGN origin, such as tidal disruption events in runaway collapsing clusters (J. Bellovary 2025). The upcoming JWST GO programs, e.g., COSMOS-3D and NEXUS, provide an excellent opportunity to investigate the LRDs' variability soon. COSMOS-3D (GO-5893) will provide one additional epoch of JWST/F115W imaging on top of COSMOS-Web (GO-1727) footprint in COSMOS field; NEXUS (GO-5105) will map around the North Ecliptic Pole with wavelength coverage 0.9–12 $\mu$m with three epochs. Both surveys will contribute a total of ~0.4 deg$^2$ area, the largest JWST multiepoch data sets exist for variable AGN studies. The methodology of this study will extend in the future to include those surveys.

## 4. Conclusion

In this study, we constrain the fraction of AGN contribution in LRDs using rest-UV variability. Our sample consists of 22 bright LRDs selected from the public JWST extragalactic field surveys, photometrically selected through V-shaped SEDs. Our study uses both HST and JWST observations in the same field coverage, taking advantage of a long time span to measure the variability of LRDs. We find a $\sim 0.15 \pm 0.26$ magnitude change spanning 6–11 yr in the rest-frame UV. We find no source with $3\sigma$ variability using both direct photometry and

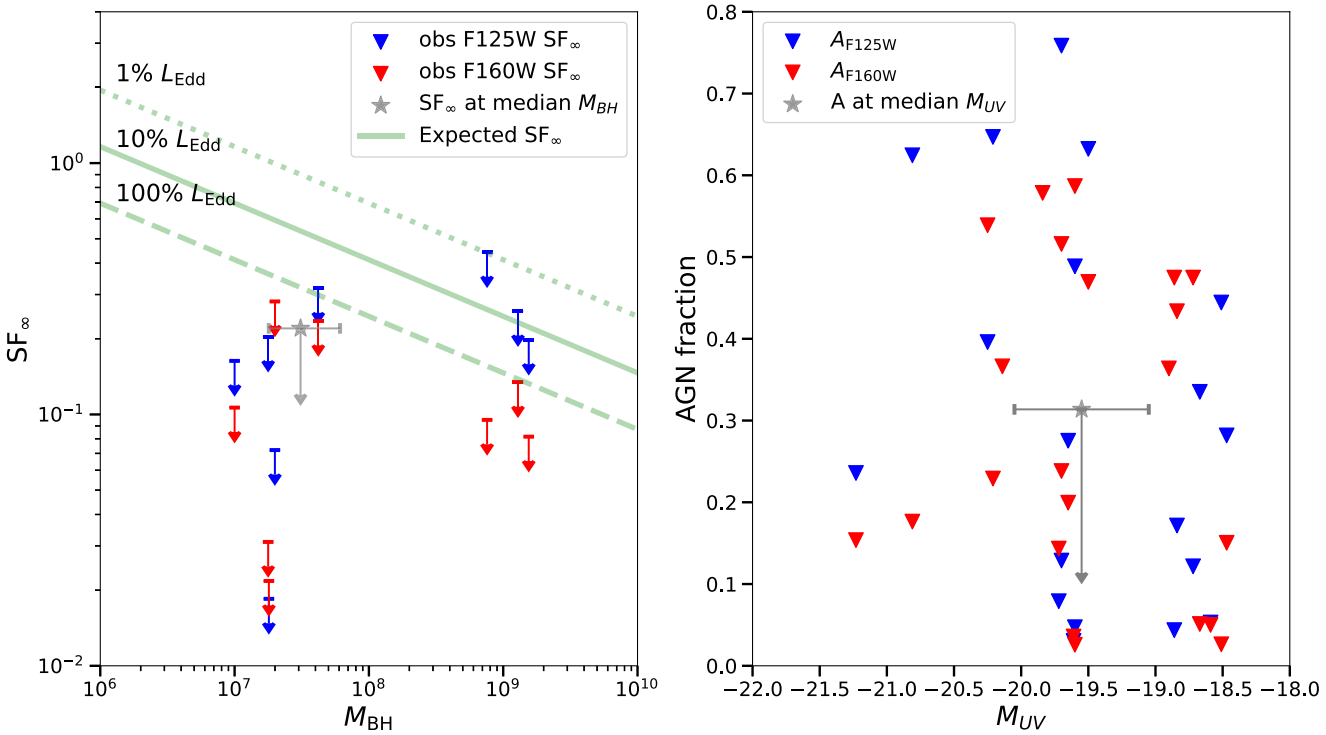


**Figure 3.** $SF_\infty$ as a function of $M_{BH}$ (left) and AGN fraction as a function of $M_{UV}$ (right). The asymptotic variability amplitude is derived from the maximum magnitude change between the HST and JWST epochs in HST/F125W and HST/F160W. The green line illustrates the asymptotic variability amplitude extrapolated from the SDSS quasar relation from C. L. MacLeod et al. (2010). The AGN fraction is a first-order estimation of the AGN flux contribution to the magnitude change, $A = \frac{SF_{\infty,d}}{SF_\infty}$; the mean of 22 LRDs results in an upper limit of 30% UV flux that is AGN-dominated.

imaging difference techniques. We derive the expected variability amplitude of LRDs by extrapolation from SDSS-like luminous AGNs, and estimate the AGN fraction by comparing the observed variability amplitude to the prediction. Our result suggests that AGN contributes $\lesssim$30% in the total UV light. Our results are consistent with the scenario that the blue UV continuum is not dominated by the AGN contributions.

## Acknowledgments

W.L.T. appreciate the comments and suggestions from J. Lyu, J. Helton, F. Sun, Y. Wu, Z. Ji, Z. Chen, X. Jin, C. Burke, J. Champagne, M. Pudoka, W. Liu, H. Zhang, C. DeCoursey, X. Lin, Y. Zhu, and M. Rieke for useful and informative discussion. W.L.T. appreciates G. Hosseinzadeh's help with imaging difference. W.L.T. and X.F. acknowledge support from HST-AR-17565. F.W. acknowledges support from NSF grant AST-2308258. W.L.T. would like to thank the support by Lia YCC throughout the work.

*Software:* Astropy (Astropy Collaboration et al. 2013, 2018, 2022), Numpy (S. van der Walt et al. 2011; C. R. Harris et al. 2020), Scipy (P. Virtanen et al. 2020), Photoutils (L. Bradley et al. 2025), PyZOGY (B. Zackay et al. 2016; D. Guevel et al. 2021).

## ORCID iDs

Wei Leong Tee https://orcid.org/0000-0003-0747-1780
Xiaohui Fan https://orcid.org/0000-0003-3310-0131
Feige Wang https://orcid.org/0000-0002-7633-431X
Jinyi Yang https://orcid.org/0000-0001-5287-4242

## References

Astropy Collaboration, Price-Whelan, A. M., Lim, P. L., et al. 2022, ApJ, 935, 167
Astropy Collaboration, Price-Whelan, A. M., Sipőcz, B. M., et al. 2018, AJ, 156, 123
Astropy Collaboration, Robitaille, T. P., Tollerud, E. J., et al. 2013, A&A, 558, A33
Bagley, M. B., Finkelstein, S. L., Koekemoer, A. M., et al. 2023, ApJL, 946, L12
Bellovary, J. 2025, arXiv:2501.03309
Bezanson, R., Labbe, I., Whitaker, K. E., et al. 2024, ApJ, 974, 92
Bradley, L., Sipőcz, B., Robitaille, T., et al. 2025, astropy/photutils: v2.1.0, Zenodo, doi:10.5281/zenodo.596036
Burke, C. J., Shen, Y., Blaes, O., et al. 2021, Sci, 373, 789
Burke, C. J., Shen, Y., Liu, X., et al. 2023, MNRAS, 518, 1880
Dayal, P., Volonteri, M., Choudhury, T. R., et al. 2020, MNRAS, 495, 3065
DeCoursey, C., Egami, E., Pierel, J. D. R., et al. 2025, ApJ, 979, 250
Durodola, E., Pacucci, F., & Hickox, R. C. 2024, arXiv:2406.10329
Eisenstein, D. J., Johnson, B. D., Robertson, B., et al. 2023, arXiv:2310.12340
Fan, X., Bañados, E., & Simcoe, R. A. 2023, ARA&A, 61, 373
Finkelstein, S., Bagley, M., & Yang, G. 2023, Data from The Cosmic Evolution Early Release Science Survey (CEERS), STScI/MAST, doi:10.17909/z7p0-8481
Finkelstein, S. L., D'Aloisio, A., Paardekooper, J.-P., et al. 2019, ApJ, 879, 36
Furtak, L. J., Secunda, A. R., Greene, J. E., et al. 2025, arXiv:2502.07875
Greene, J. E., Labbe, I., Goulding, A. D., et al. 2024, ApJ, 964, 39
Grogin, N. A., Kocevski, D. D., Faber, S. M., et al. 2011, ApJS, 197, 35
Guevel, D., Hosseinzadeh, G., Bostroem, A., & Burke, C. J. 2021, dguevel/PyZOGY: v0.0.2, Zenodo, doi:10.5281/zenodo.4570234
Habouzit, M., Onoue, M., Bañados, E., et al. 2022, MNRAS, 511, 3751
Harikane, Y., Ouchi, M., Oguri, M., et al. 2023b, ApJS, 265, 5
Harikane, Y., Zhang, Y., Nakajima, K., et al. 2023a, ApJ, 959, 39
Harris, C. R., Millman, K. J., van der Walt, S. J., et al. 2020, Natur, 585, 357
Hayes, M. J., Tan, J. C., Ellis, R. S., et al. 2024, ApJL, 971, L16
Illingworth, G., Magee, D., Bouwens, R., et al. 2016, arXiv:1606.00841
Inayoshi, K., & Ichikawa, K. 2024, ApJL, 973, L49
Inayoshi, K., Nakatani, R., Toyouchi, D., et al. 2022, ApJ, 927, 237

Jeon, J., Bromm, V., Liu, B., & Finkelstein, S. L. 2025, ApJ, 979, 127
Killi, M., Watson, D., Brammer, G., et al. 2024, A&A, 691, A52
Kocevski, D. D., Finkelstein, S. L., Barro, G., et al. 2024, arXiv:2404.03576
Kocevski, D. D., Onoue, M., Inayoshi, K., et al. 2023, ApJL, 954, L4
Koekemoer, A. M., Faber, S. M., Ferguson, H. C., et al. 2011, ApJS, 197, 36
Kokorev, V., Caputi, K. I., Greene, J. E., et al. 2024, ApJ, 968, 38
Kokubo, M., & Harikane, Y. 2024, arXiv:2407.04777
Kozłowski, S. 2016, ApJ, 826, 118
Labbe, I., Greene, J. E., Bezanson, R., et al. 2025, ApJ, 978, 92
Li, Z., Inayoshi, K., Chen, K., Ichikawa, K., & Ho, L. C. 2025, ApJ, 980, 36
MacLeod, C. L., Ivezić, Ž., Kochanek, C. S., et al. 2010, ApJ, 721, 1014
MacLeod, C. L., Ivezić, Ž., Sesar, B., et al. 2012, ApJ, 753, 106
Maiolino, R., Risaliti, G., Signorini, M., et al. 2024b, MNRAS, 538, 1921
Maiolino, R., Scholtz, J., Curtis-Lake, E., et al. 2024a, A&A, 691, A145
Matthee, J., Naidu, R. P., Brammer, G., et al. 2024, ApJ, 963, 129
O'Brien, R., Jansen, R. A., Grogin, N. A., et al. 2024, ApJS, 272, 19
Pacucci, F., Nguyen, B., Carniani, S., Maiolino, R., & Fan, X. 2023, ApJL, 957, L3
Richards, G. T., Strauss, M. A., Fan, X., et al. 2006, AJ, 131, 2766
Rieke, M., Robertson, B., Tacchella, S., et al. 2023, Data from the JWST Advanced Deep Extragalactic Survey (JADES), STScI/MAST, doi:10.17909/8tdj-8n28
Sánchez, P., Lira, P., Cartier, R., et al. 2017, ApJ, 849, 110
Shen, Y., Strauss, M. A., Ross, N. P., et al. 2009, ApJ, 697, 1656
Simm, T., Salvato, M., Saglia, R., et al. 2016, A&A, 585, A129
Suess, K. A., Weaver, J. R., Price, S. H., et al. 2024, ApJ, 976, 101
Turner, T. J., George, I. M., Nandra, K., & Turcan, D. 1999, ApJ, 524, 667
van der Walt, S., Colbert, S. C., & Varoquaux, G. 2011, CSE, 13, 22
Vanden Berk, D. E., Wilhite, B. C., Kron, R. G., et al. 2004, ApJ, 601, 692
Virtanen, P., Gommers, R., Oliphant, T. E., et al. 2020, NatMe, 17, 261
Weaver, J. R., Cutler, S. E., Pan, R., et al. 2024, ApJS, 270, 7
Whitaker, K. E., Ashas, M., Illingworth, G., et al. 2019, ApJS, 244, 16
Williams, C., Tacchella, S., Maseda, M., et al. 2023, Data from the JWST Extragalactic Medium-band Survey (JEMS), STScI/MAST, doi:10.17909/fsc4-dt61
Yue, M., Eilers, A.-C., Ananna, T. T., et al. 2024, ApJL, 974, L26
Yung, L. Y. A., Somerville, R. S., Finkelstein, S. L., et al. 2021, MNRAS, 508, 2706
Zackay, B., Ofek, E. O., & Gal-Yam, A. 2016, ApJ, 830, 27
Zhang, Z., Jiang, L., Liu, W., & Ho, L. C. 2024, arXiv:2411.02729